COMMUNICATION

Organolead Halide Perovskites for Low Operating Voltage Multilevel Resistive Switching

Jaeho Choi, Sunghak Park, Joohee Lee, Kootak Hong, Do-Hong Kim, Cheon Woo Moon, Gyeong Do Park, Junmin Suh, Jinyeon Hwang, Soo Young Kim, Hyun Suk Jung, Nam-Gyu Park, Seungwu Han, Ki Tae Nam,* and Ho Won Jang*

Organolead halide perovskites (OHPs) with the chemical formula ABX_3 consist of a 3D connected network of corner-sharing lead halide octahedral. Organic cations, such as methylammonium or formamidinium occupy the cubo-octahedral sites, which are each shared by twelve halide anions. Due to their inherent hybrid structure, OHPs show unusual electrical and optical properties such as high light absorption and structural and compositional flexibility.[1–4] Mixed ionic–electronic conduction behavior is found in OHPs, suggesting ion migration plays a role in devices based on the materials. Methylammonium lead iodide ($CH_3NH_3PbI_3$) has received attention as a light absorber[5–7] and charge transport[8,9] material for solar cells. Its superior properties, such as a large light absorption coefficient, a small exciton binding energy,[10] and a balanced long-range charge diffusion length,[11] make the material ideal for photovoltaic applications.

Here, we report an ultralow electric field and high ON/OFF ratio resistive switching behavior of solution-processed OHP films, which is exploited for multilevel data storage. $Ag/CH_3NH_3PbI_3/Pt$ cells exhibit electroforming-free resistive switching at an electric field of 3.25×10^3 V cm^{-1} for distinguishable four ON-state resistance levels. Density functional theory calculations show that the migration of iodine interstitials and vacancies with low activation energies is responsible for the low electric field resistive switching via filament formation and annihilation.

One of the interesting phenomena that inspired this study is the hysteretic current–voltage characteristics exhibited by $CH_3NH_3PbI_3$ due to the build-up of space charges close to the contacts originating from ionic displacement.[12,13] Xiao et al.[12] showed that photocurrent direction in $CH_3NH_3PbI_3$ films could be switched repeatedly by applying a small electric field of <1 V μm^{-1}, which was explained by the formation of reversible p–i–n structures induced by ion drift in the perovskite layer. Although the exact defect nature is still elusive, recent studies have shown that negatively charged Pb and CH_3NH_3 vacancies and positively charged I vacancies are the predominant ionic species.[14,15] More excitingly, the rotational motion of the A-site organic cation can provide structural flexibility and even ferroelectric behavior on the nanoscale.[16,17] **Figure 1**a depicts the rotational motion of the CH_3NH_3 cation in the unit cell of $CH_3NH_3PbI_3$. Unlike the spherical Pb cation and I anion, the MA cation is asymmetric dumbbell-shaped. At the ground state, the CH_3NH_3 cation tilts toward the diagonal direction by ≈30°.[17,18] Since the molecule is polar, the CH_3NH_3 cation may rotate with an external electric field. Especially, when the external electric field is applied along the c-axis, the CH_3NH_3 cation can rotate and align with the external bias. For the room temperature cubic phase of $CH_3NH_3PbI_3$, the fast rotational dynamics of the CH_3NH_3 cations in picosecond time scale was predicted.[19,20] Such a molecular rotational motion can lead to lowering the barrier for the migration of point defects including vacancies and interstitials. This unique nature of $CH_3NH_3PbI_3$ motivated us to explore whether the OHP can be used as a resistive switching material, where the electrochemical motion of the charged ions and/or the structural phase transition play a role.[21–25]

Here, we report extraordinary resistive switching behavior of organic–inorganic hybrid perovskite thin films under extremely low electric fields. Typical I–V characteristics of solution-processed 400-nm-thick $CH_3NH_3PbI_3$ thin films sandwiched with Ag top and Pt bottom electrodes exhibit resistive switching with ON/OFF ratio greater than 10^6 and SET voltages (to a low resistance state) below 0.15 V, leading to demonstrating four-level resistance states for multilevel data storage. We performed first-principles calculations to describe the ultralow electric field bipolar resistive switching properties of the $CH_3NH_3PbI_3$ thin films.

The $CH_3NH_3PbI_3$ thin films used for this study were 400 nm thick and the average grain size was ≈133 nm, as shown in Figure S1 (Supporting Information). Despite a large variation in grain size, the $CH_3NH_3PbI_3$ thin films were uniformly spin-coated on $Pt/Ti/SiO_2/Si$ substrates. Figure 1b shows that the $CH_3NH_3PbI_3$ thin film is polycrystalline and of a single-phase organolead halide as shown in the X-ray diffraction pattern in

J. Choi, S. Park, J. Lee, K. Hong, D.-H. Kim,
C. W. Moon, G. D. Park, J. Suh, J. Hwang, Prof. S. Han,
Prof. K. T. Nam, Prof. H. W. Jang
Department of Materials Science and Engineering
Seoul National University
Seoul 08826, Republic of Korea
E-mail: nkitae@snu.ac.kr; hwjang@snu.ac.kr

Prof. S. Y. Kim
School of Chemical Engineering and Materials Science
Chung-Ang University
Seoul 06974, Republic of Korea

Prof. H. S. Jung
School of Advanced Materials Science and Engineering
Sungkyunkwan University
Suwon 16419, Republic of Korea

Prof. N.-G. Park
School of Chemical Engineering and Department of Energy Science
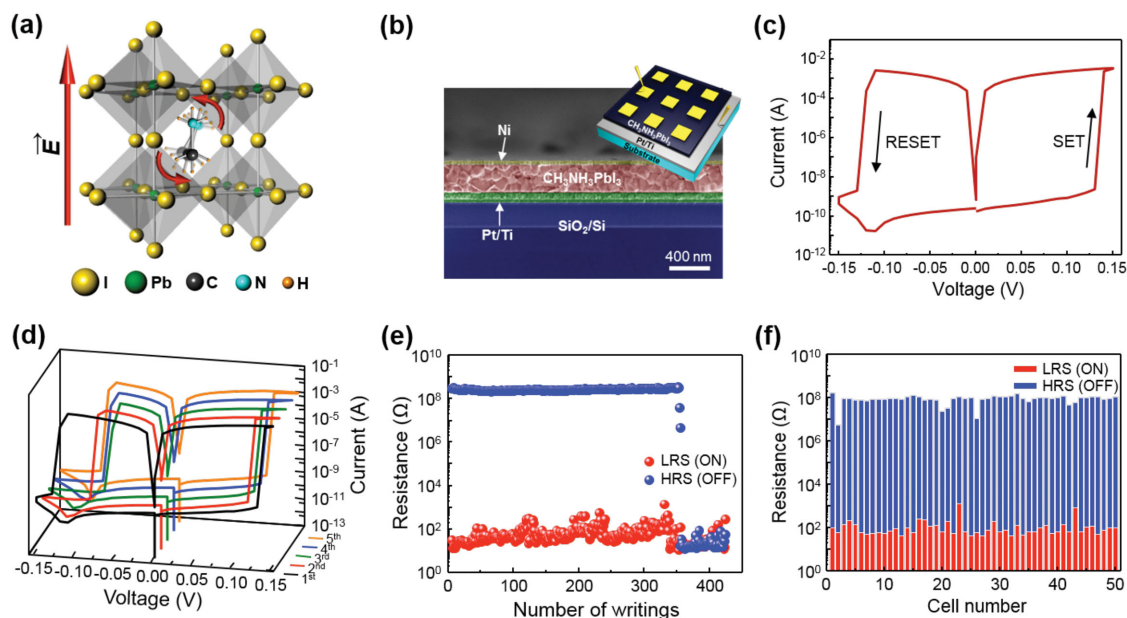Sungkyunkwan University
Suwon 16419, Republic of Korea

Figure 1. Resistive switching properties of Ag/CH₃NH₃PbI₃/Pt cells. a) A-site molecular rotational motion in a unit cell of $CH_3NH_3PbI_3$. b) Cross-sectional SEM image of a fabricated Ni/CH₃NH₃PbI₃/Pt/Ti/SiO₂/Si vertical structure and schematic of the metal/ $CH_3NH_3PbI_3$/metal vertical structure for resistive switching (inset). c) Typical current–voltage (I–V) characteristic of Ag/CH₃NH₃PbI₃/Pt cells. d) I–V characteristics of a Ag/CH₃NH₃PbI₃/ Pt cell from five initial voltage sweeps. SET voltage is +0.15 V and RESET voltage is −0.15 V. e) Reversible resistive switching measured with a writing voltage of 0.15 V and a reading voltage of 0.02 V. The pulse width of the writing voltage was 200 ms. f) High and low resistance states for 50 different cells. The average on/off ratio is calculated to be 1.12×10^6.

Figure S1 (Supporting Information).[17] After spin-coating and annealing of the CH₃NH₃PbI₃ thin film, metal-insulator-metal (MIM) vertical structure cells were fabricated by depositing 50 μm × 50 μm top metal electrodes such Ag, Ni, and Au using a shadow mask and an electron beam evaporator. To achieve pinhole-free CH₃NH₃PbI₃ films with uniform thicknesses we used a rapid crystallization method using N,N-dimethylfor-mamide and toluene as the solvent for the OHP precursors (CH₃NH₃I and PbI₂). Because CH₃NH₃PbI₃ and the precursors are minimally soluble in toluene, the addition of toluene significantly reduced the solubility of CH₃NH₃PbI₃ in the mixed solution and rapid crystallization occurred. As a result of the rapid crystallization, we obtained uniform and pinhole-free CH₃NH₃PbI₃ films.[26] Using the pinhole-free MIM cells (Figure 1b; Figure S2, Supporting Information), we succeeded in measuring insulating ground states from the solution-processed CH₃NH₃PbI₃ films.

A typical I–V curve of the Ag/CH₃NH₃PbI₃/Pt cells is shown in Figure 1c. With the applied voltage sweep of 0 V → +0.15 V → 0 V → −0.15 V → 0 V, the measured current values were plotted on a logarithmic scale. The hysteresis loop indicates that the device exhibits bipolar switching.[21,27] Initially, the device was in an insulating (high resistance) state (HRS) with current levels of 10^{-10}–10^{-9} A. The devices with both thin and thick CH₃NH₃PbI₃ films also show low current levels of 10^{-10}–10^{-9} A. These low current levels support that the solution-processed CH₃NH₃PbI₃ films are pinhole-free. The current increases abruptly when the applied voltage is ≈0.13 V. Then, the device retained a conducting (low resistance) state (LRS) with current levels near 10^{-3} A. It should be noted that the current density for the LRS state is over hundreds of times higher than the

photocurrent densities of the CH₃NH₃PbI₃ films studied for photovoltaic applications. The equivalent electric field for the onset of the low resistance state is 3.25×10^3 V cm⁻¹ for the 400 nm thick CH₃NH₃PbI₃ film. The transition between HRS (OFF state) and LRS (ON state) is switchable and the ON/OFF ratio is as high as ≈10⁶. The CH₃NH₃PbI₃ devices do not require electroforming, even though the thickness of the CH₃NH₃PbI₃ thin film is ≈400 nm. In Figure 1d, The I–V curves do not show remarkable variation in the SET voltages, indicating the electroforming-free characteristic of the CH₃NH₃PbI₃-based MIM cells. It is interesting that the operation electric field (3.75×10^3 V cm⁻¹) is comparable to the applied electric field for the switchable photovoltaic effect in CH₃NH₃PbI₃–based devices (1.2×10^4 V cm⁻¹), where the electrical programming with optical reading out was explained by the migration of defect ions. It was observed that the SET voltages of the Ag/CH₃NH₃PbI₃/Pt cells can be even lower with the slower scan rates (Figure S3, Supporting Information). When the thickness of the CH₃NH₃PbI₃ film was reduced to 220 nm, the SET voltage decreased to 0.11 V, while the SET voltage was as high as 0.55 V for the 1.1 μm thick CH₃NH₃PbI₃ film (Figure S4, Supporting Information).

Resistive switching with voltage pulses is also possible for the device (Figure 1e). At voltages of ±0.15 V (200 ms pulse width), the CH₃NH₃PbI₃-based MIM cell showed reproducible resistive switching with ON/OFF ratios above 10⁶ over 350 cycles. The typical retention characteristics of the ON and OFF states for an Ag/CH₃NH₃PbI₃/Pt cell showed that the ON state is stable up to 11 000 s (Figure S5, Supporting Information). Since the switching voltage (±0.15 V) is low, the thermal voltage at room temperature (0.025 V) can disturb the ON state,

making the retention time of the ON state short. We measured 50 $Ag/CH_3NH_3PbI_3/Pt$ cells for resistive switching with writing voltages of ± 0.15 V (250 ms pulse width). As plotted in Figure 1f, the 50 electrodes showed an average ON/OFF ratio of 1.12×10^6 without considerable deviations. The reproducibility of the uniform HRS and LRS levels of many cells indicates that the $CH_3NH_3PbI_3$-based MIM cells are feasible for reliably high ON/OFF ratio resistive switching with a low electric field. To obtain the HRS states, the ratio of methylammonium iodide (MAI) and lead iodide (PbI_2) precursors should be controlled to be 1:1. When the MAI/PbI_2 ratio is 1.05 or 0.95, the $CH_3NH_3PbI_3$ thin films were metallic and hysteretic I–V characteristics could not be obtained (Figure S6, Supporting Information).

To understand the current conduction mechanism at the interface between the top electrode and the $CH_3NH_3PbI_3$ layer, we highlighted the I–V curves for the ON and OFF states of the $Ag/CH_3NH_3PbI_3/Pt$ and $Ni/CH_3NH_3PbI_3/Pt$ cells (Figure S7, Supporting Information). For both cells which adopted Ag and Ni top electrodes, the OFF state I–V curves show linear and nonlinear regions, indicating that space-charge limited conduction is dominant. The ON state I–V curves exhibit perfect ohmic behavior, suggesting the formation of highly conducting paths between the top and bottom electrodes. The dependence of the current levels for the ON and OFF states of $Ag/CH_3NH_3PbI_3/Pt$ cells on the area of the top electrode was investigated. Although the area of the top electrode was increased 64 fold, the current levels for the ON states did not increase, whereas the current levels for the OFF states varied considerably at the nA scale. This result indicates that the conducting paths for the ON states are localized, namely, filamentary.[21,22,28,29] Ag is known to be a relatively active metal than Ni and Au. MIM cells with Ag top electrodes showed operation voltages less than ± 0.14 V, whereas cells with Ni and Au top electrodes showed higher operation voltages over ± 0.4 V. It is suggested that the electrochemical activity of the top electrode plays a role in triggering the abrupt resistive switching behavior.

We performed conducting atomic force microscopy (CAFM) on a $CH_3NH_3PbI_3$ film on $Ag/Ti/SiO_2$ substrate in order to determine whether the preexisting grain boundaries or non-uniformity in the thickness play a role in forming conducting filaments for the ON states, as shown in **Figure 2**. The 400 nm thick film was granular. The grain size varied from 300 to 1000 nm and the rms roughness is about 40 nm with a maximum peak-to-valley depth of 60 nm. At a bias of 0.1 V on the probe tip, the $CH_3NH_3PbI_3$ film was uniformly insulating with current levels of several tens of nA (Figure 2b). The film became conductive with current levels of ≈ 50 μA at a bias of 1 V (Figure 2c). The current map is quite different from the morphology map and the whole area of the film was conductive. It is suggested that conducting filaments which could not be visualized with the atomic force microscopy (AFM) tip of ≈ 50 nm radius were formed through the $CH_3NH_3PbI_3$ film under an external bias. We could vary the grain size in the $CH_3NH_3PbI_3$ film from 70 to 600 nm by controlling the annealing condition of the film (Table S2, Supporting Information). Combined with X-ray diffraction data, endurance measurements revealed that obtaining the films with the constituted composition without secondary phases is more important than tailoring the grain size (Figures S8 and S9, Supporting Information).

To compare the extraordinary resistive switching properties of the $CH_3NH_3PbI_3$-based devices with those of conventional resistive switching devices, we plotted the ON/OFF ratio versus the reciprocal of the electric field for SET ($1/E_{SET}$) in **Figure 3**a.[20,29–46] Binary transition metal oxides, such as TiO_2 and TaO_x, the most widely studied materials for resistive switching, show varied ON/OFF ratios and relatively low $1/E_{SET}$ values ($< 1 \times 10^{-5}$ cm V^{-1}). Inorganic perovskites, such as $SrTiO_3$, exhibit low $1/E_{SET}$ values near $\approx 10^{-5}$ cm V^{-1} with relatively low ON/OFF ratios. Organic materials demonstrate the lowest $1/E_{SET}$ values, showing large variations in the ON/OFF ratios. The OHP $CH_3NH_3PbI_3$ has a relatively high ON/OFF ratio of $> 10^6$ and the highest $1/E_{SET}$ value, which is one order of magnitude higher than those of chalcogenides.

We note that the formation of conducting filaments is by Ag migration, though the 400 nm thick $CH_3NH_3PbI_3$ film is rare for an SET voltage as low as 0.13 V, which corresponds to 3.25×10^3 V cm^{-1}. Conventional Ag migration resistive switching memories typically require much higher electric fields for SET ($> 1 \times 10^5$ V cm^{-1}) and undergo electroforming under even higher electric fields.[21] In addition, $Ag/CH_3NH_3PbI_3/Pt$ and $Ni/CH_3NH_3PbI_3/Pt$ cells showed similar ON/OFF ratios. This suggests that charged defect ions (point defects) in the film itself rather than metal ions are
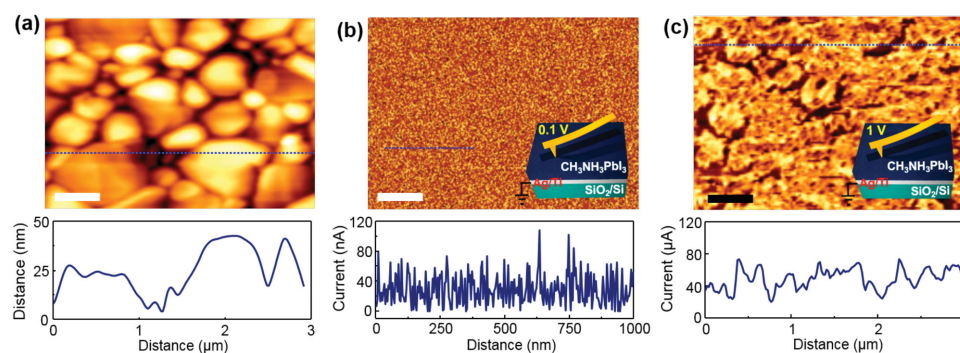

Figure 2. Scanning probe microscopy images of $CH_3NH_3PbI_3$ thin films. a) A topological AFM image of the $CH_3NH_3PbI_3/Ag$ structure. The scale of bars is 500 nm. The tip moves 3 μm through the blue dotted line to measure the roughness by the distance (down). b,c) CAFM images of a $CH_3NH_3PbI_3/Ag$ structure with platinum-coated tip biases of (b) 0.1 V and (c) 1 V. The scale of bars is 500 nm. The tip moves through the blue dotted line to measure the current versus the distance (down). It is noted that the morphology map and the current map were obtained simultaneously.
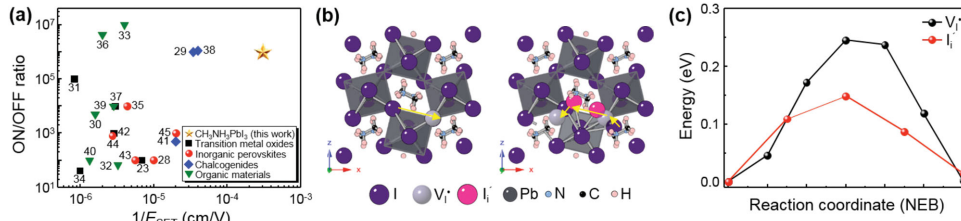
Figure 3. Comparison with various resistive switching materials and DFT calculation. a) The ON/OFF ratio of resistive switching devices including the CH$_3$NH$_3$PbI$_3$-based cells. b) Schematic migration paths of $V_I^\bullet$ (left) and $I_i^{'}$ (right) in the unit cell of CH$_3$NH$_3$PbI$_3$. The center of the split interstitial is moved to adjacent I site, and the direction of the split rotates to another [110] direction. c) DFT calculation about the activation energy for the movements of $V_I^\bullet$ and $I_i^{'}$ to the next sites.

responsible for the ultralow electric field resistive switching via the formation of conducting filaments.[21,22,24] To reveal the origin of the resistive switching in the CH$_3$NH$_3$PbI$_3$-based cells, we studied the migration energies of representative point defects in CH$_3$NH$_3$PbI$_3$ with density functional theory (DFT) calculations, assuming that the hysteretic $I–V$ characteristics are caused by the migration of charged point defects.[47–51] CH$_3$NH$_3$PbI$_3$ has abundant, intrinsic, shallow point defects. We consider two point defects, $V_I^\bullet$ and $I_i^{'}$ (split interstitial), which are thermodynamically stable and likely to be highly mobile.[8,9,12,17,52] The generalized gradient approximation functional is adopted and the migration barrier is calculated using the nudged elastic band method. As shown in Figure 3b,c and Figure S11 (Supporting Information), $V_I^\bullet$ and $I_i^{'}$ can migrate with low activation energies of 0.25 and 0.15 eV, respectively. These energies are significantly lower than the migration barriers of $V_O^{\bullet\bullet}$ in TiO$_2$ (1.15 eV) and SrTiO$_3$ (1.22 eV) which are widely used in resistive switching devices (Figure S11, Supporting Information).[53,54] Therefore, we suggest that the low switching voltages of the CH$_3$NH$_3$PbI$_3$ cells are due to the small migration barriers of the charged anion defects. To provide plausible explanation for the resistive switching in the Ag/CH$_3$NH$_3$PbI$_3$/Pt cells, we illustrated the procedure of filament formation and annihilation due to the migration of $I_i^{'}$ (Figure S12, Supporting Information). The filament consisting of $I_i^{'}$ can be an iodine-rich secondary phase that is metallic or a degenerated semiconductor by the accumulation of compensating holes for charge neutrality. However, further studies are necessary to find the exact mechanism. Since $I_i^{'}$ and $V_I^\bullet$ are

oppositely charged each other, the unintentional migration of $V_I^\bullet$ can rupture the conducting filaments, which was formed by the aggregation of $I_i^{'}$. Thus, obtaining CH$_3$NH$_3$PbI$_3$ films with similarly charged point defects is expected to be critical for reliable resistive switching performance for long-term operation. Since the migration of the defect ions could be much slowed down at lower temperatures, the filamentary resistance switching behavior deteriorated significantly at 150 and 100 K (Figure S13, Supporting Information).

Since the high ON/OFF ratio is giant and abrupt, multilevel resistive switching could be exploited for the CH$_3$NH$_3$PbI$_3$ devices. $I–V$ characteristics of the Ag/CH$_3$NH$_3$PbI$_3$/Pt cells under different compliance currents are shown in **Figure 4**a. When the compliance current was lowered from 10^{-2} and to 10^{-4} A, 10^{-5} and 10^{-6} A for the positive voltage sweep, reversible resistive switching was feasible without negligible fluctuation in the SET voltage (Figure S14, Supporting Information). The distribution of multilevel ON states upon a number of writing cycles is shown in Figure 4b. Distinguishably different resistance states can be found for compliance currents of 10^{-2}, 10^{-4}, and 10^{-5} A. However, the endurance for resistive switching with the compliance current of 10^{-6} A is relatively poor. With the lower compliance current, the endurance for reversible resistance switching is deteriorated (Figure S15, Supporting Information). This result clearly demonstrates that at least four different ON states can be achieved in the CH$_3$NH$_3$PbI$_3$ devices for the multilevel data storage by controlling the compliance current for the SET process. We believe that synthesizing thinner pinhole-free CH$_3$NH$_3$PbI$_3$ films in a reproducible
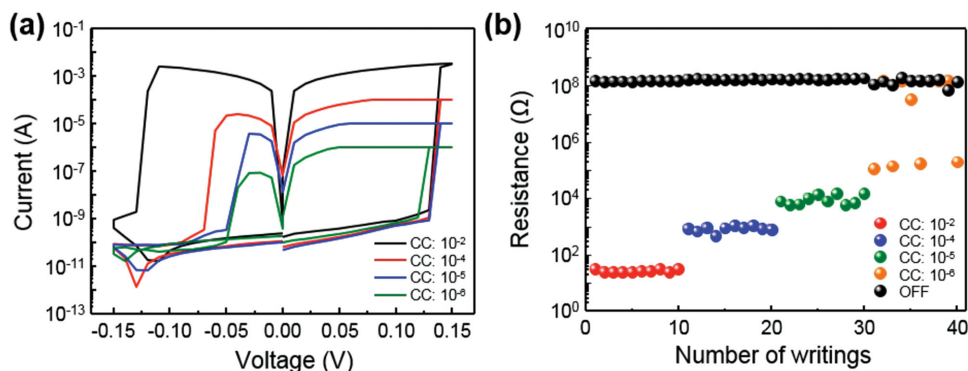

Figure 4. Multilevel resistive switching properties. a) $I–V$ characteristics of Ag/CH$_3$NH$_3$PbI$_3$/Pt cells under three different compliance currents (CC = 10^{-2}, 10^{-4}, 10^{-5}, and 10^{-6} A). b) Reversible resistive switching over 40 cycles with different current compliances of 10^{-2}, 10^{-4}, 10^{-5}, and 10^{-6} A. The switching pulse duration is fixed to 200 ms, and the switching voltage is 0.15 V.

manner, controlling the formation of native point defects, and understanding the underlying mechanisms exactly are urgently needed for improving endurance and retention properties of $CH_3NH_3PbI_3$-based resistive switching cells for real applications to data storage and minimizing the cell-to-cell variation for reliable operation, which will pave the way for a new material platform in developing high performance nonvolatile memories.

In conclusion, we demonstrated multilevel resistive switching using an OHP. Solution-processed 400 nm thick $CH_3NH_3PbI_3$ films with Ag top and Pt bottom electrodes exhibited electroforming-free resistive switching with a low SET voltage of ≈0.13 and high ON/OFF ratios of ≈10^6 under ±0.15 V pulses. Based on these extraordinary properties, four-level storage capability of the $CH_3NH_3PbI_3$-based devices was demonstrated. We attributed the high performance resistive switching behavior of the $CH_3NH_3PbI_3$-based devices to the energetically benign migration of anions defects ($V_I^{\bullet}$ and I_I'), but further studies are needed to identify the mechanism responsible for the ultralow electric field resistive switching. Enhancements in switching speed, endurance, and retention are also necessary and may be achieved by controlling the doping concentration, crystallinity, and large area compositional uniformity of the OHP film. The inherent structural flexibility and the number of possible combinations for ABX_3-type OHPs will support intensive studies for other electronic device applications beyond resistive switching memories. Finally, we believe that the solution-processed $CH_3NH_3PbI_3$-based cells are promising for microelectronics built on flexible substrates.

Experimental Section

Materials Preparation: Methylammonium iodide (CH_3NH_3I) was prepared by reacting methylamine (7.46 mL, 40% in methanol, TCI) and hydriodic acid (10 mL, 55% in water, ACROS ORGANICS). Reacting solution was stirred at 0 °C for 2 h. The solvent was removed by rotary evaporation at 50 °C for 1 h. The precipitate (CH_3NH_3I) was dissolved in ethanol and mixing diethyl ether (Daejung Chemicals) for recrystallization. This recrystallization process was repeated twice. After recrystallization, product (CH_3NH_3I) dried in vacuum oven at 60 °C for 24 h.

Film Formation and MIM Cell Fabrication: Pt/Ti-coated substrates were prepared by electron beam evaporation. First, a 20 nm thick Ti thin film was deposited on SiO_2 substrates using e-beam evaporator for the better adhesion of the Pt layer and a 50 nm thick Pt thin film was sequently deposited on the substrates. The Pt-coated substrates were washed by acetone, isopropanol, and deionized water under ultrasonication and then treated by air plasma cleaner for 5 min just prior to the synthesis of $CH_3NH_3PbI_3$ films on the substrates. $CH_3NH_3PbI_3$ films were synthesized on Pt/Ti/SiO_2/Si substrates. The perovskite precursor solution was prepared by MAI powders and PbI_2 in various molar ratios (MAI/ PbI_2 ratios from 0.9 to 1.1) in anhydrous *N*,*N*-dimethylformamide for overall concentration of 40 wt%. To deposit $CH_3NH_3PbI_3$ perovskite film, the resulting solution was spin-coated on Pt/Ti/SiO_2/Si and glass substrates at 4000 rpm for 60 s. During the spin coating (5 s after spinning), anhydrous toluene was dropped onto the center of the substrate for better morphology of $CH_3NH_3PbI_3$ perovskite film. After spin coating, film was annealed on a hot plate at 70 °C for 30 min. Ag, Ni, and Au were selected as top electrodes of resistive switching device. 50 μm × 50 μm, 200 μm × 200 μm, and 400 μm × 400 μm of top electrodes were deposited on $CH_3NH_3PbI_3$

perovskite film by e-beam evaporation method with the shadow mask. The evaporation was performed at 1×10^{-6} Torr of pressure and room temperature.

Device Characterization: For X-ray diffraction (XRD) measurements, a $CH_3NH_3PbI_3$ perovskite film was coated on a glass substrate. The XRD pattern was obtained from X-Ray Diffractometer (BRUKER MILLER Co., D8-Advance) with Cu Kα radiation (λ = 1.54056 Å). XRD data were recorded at room temperature in the range of 10°–60° of 2θ range with a step size of 0.02° and scan speed of 2° min^{-1}. The surface and cross-sectional images were obtained from field emission scanning electron microscope (ZEISS, MERLIN Compact). Images were obtained with an in-lens secondary electron detector at 1 kV accelerating voltage. The *I–V* characteristics were measured by Agilent 4156C semiconductor analyzer with direct current voltage sweeping mode. Resistive switching by alternating voltage pulses was measured by the Agilent 4156C semiconductor analyzer. All of the electrical properties were measured in a vacuum chamber (6×10^{-2} Torr). To observe conduction mechanism in the $CH_3NH_3PbI_3$ films, the conductance of $CH_3NH_3PbI_3$ films coated on Ag/Ti/SiO_2/Si substrate at room temperature was measured by CAFM (Park systems XE100) in a glovebox, which was Ar atmosphere. A platinum-coated STM-type tip was used to substitute platinum counter electrodes.

DFT Calculation: The first-principles DFT calculations based on the projected augmented wave pseudopotential were performed using the Vienna ab initio simulation package code. The nudged elastic band method was employed in computing the activation energy along the migration path. As the present DFT study assumes the 0 K temperature condition, the orthorhombic phase of the $CH_3NH_3PbI_3$ was used for the calculation. The supercell includes 48 atoms (orthorhombic unit cell) for the iodine vacancy and 182 atoms ($2 \times 2 \times 1$ orthorhombic cell) for the interstitial iodine. The cutoff energy for plane-wave basis set was chosen to be 550 eV and the gamma point was sampled in the Brillouin-zone integration. Atomic positions were relaxed until the forces were reduced below 0.02 eV $Å^{-1}$.

Supporting Information

Supporting Information is available from the Wiley Online Library or from the author.

Acknowledgements

[1] D. B. Mitzi, S. Wang, C. A. Field, C. A. Chess, A. M. Guloy, *Science* **1995**, *267*, 1473.

[2] D. B. Mitzi, K. Chondroudis, C. R. Kagan, *Inorg. Chem.* **1999**, *38*, 6246.

[3] N. J. Jeon, J. H. Noh, W. S. Yang, Y. C. Kim, S. Ryu, J. Seo, S. I. Seok, *Nature* **2015**, *517*, 476.

[4] G. E. Eperon, S. D. Stranks, C. Menelaou, M. B. Johnston, L. M. Herz, H. J. Snaith, *Energy Environ. Sci.* **2014**, *7*, 982.

[5] W. J. Yin, T. Shi, Y. Yan, *Adv. Mater.* **2014**, *26*, 4653.

[6] H. S. Kim, C. R. Lee, J. H. Im, K. B. Lee, T. Moehl, A. Marchioro, R. Humphry-Baker, J. H. Yum, J. E. Moser, M. Grätzel, N. G. Park, *Sci. Rep.* **2012**, *2*, 591.

[7] J. H. Im, C. R. Lee, J. W. Lee, S. W. Park, N. G. Park, *Nanoscale* **2011**, *3*, 4088.

[8] M.-H. Du, *J. Mater. Chem. A* **2014**, *2*, 9091.

[9] C. Eames, J. M. Frost, P. R. F. Barnes, B. C. O'Regan, A. Walsh, M. S. Islam, *Nat. Commun.* **2015**, *6*, 7497.

[10] K. Tanaka, T. Takahashi, T. Ban, T. Kondo, K. Uchida, N. Miura, *Solid State Commun.* **2003**, *127*, 619.

[11] G. Xing, N. Mathews, S. Sun, S. S. Lim, Y. M. Lam, M. Grätzel, S. Mhaisalkar, T. C. Sum, *Science* **2013**, *342*, 344.

[12] Z. Xiao, Y. Yuan, Y. Shao, Q. Wang, Q. Dong, C. Bi, P. Sharma, A. Gruverman, J. Huang, *Nat. Mater.* **2015**, *14*, 193.

[13] W. Tress, N. Marinova, T. Moehl, S. M. Zakeeruddin, M. K. Nazeeruddin, M. Grätzel, *Energy Environ. Sci.* **2015**, *8*, 995.

[14] J. Kim, S.-H. Lee, J. H. Lee, K.-H. Hong, *J. Phys. Chem. Lett.* **2014**, *5*, 1312.

[15] W. J. Yin, T. T. Shi, Y. F. Yan, *Appl. Phys. Lett.* **2014**, *104*, 063903.

[16] A. Poglitsch, D. Weber, *J. Chem. Phys.* **1987**, *87*, 6373.

[17] C. C. Stoumpos, C. D. Malliakas, M. G. Kanatzidis, *Inorg. Chem.* **2013**, *52*, 9019.

[18] Y. Kawamura, H. Mashiyama, K. Hasebe, *J. Phys. Soc. Jpn.* **2002**, *71*, 1694.

[19] R. Gottesman, E. Haltzi, L. Gouda, S. Tirosh, Y. Bouhadana, A. Zaban, *J. Phys. Chem. Lett.* **2014**, *5*, 2662.

[20] Q. Lai, Z. Zhu, Y. Chen, S. Patil, F. Wudl, *Appl. Phus. Lett.* **2006**, *88*, 133513.

[21] R. Waser, R. Dittmann, G. Staikov, K. Szot, *Adv. Mater.* **2009**, *21*, 2632.

[22] F. Pan, S. Gao, C. Chen, C. Song, F. Zeng, *Mater. Sci. Eng. R-Rep.* **2014**, *83*, 1.

[23] I. Valov, R. Waer, J. R. Jameson, M. N. Kozicki, *Nanotechnology* **2011**, *22*, 254003.

[24] R. Waser, M. Aono, *Nat. Mater.* **2007**, *6*, 833.

[25] E. J. Yoo, M. Lyu, J. H. Yun, C. J. Kang, Y. J. Choi, L. Wang, *Adv. Mater.* **2015**, *27*, 6170.

[26] M. Xiao, F. Huang, W. Huang, Y. Dkhissi, Y. Zhu, J. Etheridge, A. Gray-Weale, U. Bach, Y.-B. Cheng, L. Spiccia, *Angew. Chem.* **2014**, *126*, 10056.

[27] G. Dearnale, A. M. Stoneham, D. V. Morgan, *Rep. Prog. Phys.* **1970**, *33*, 1129.

[28] Y. Aoki, C. Wiemann, V. Feyer, H.-S. Kim, C. M. Schneiger, H. Ill-Yoo, M. Martin, *Nat. Commun.* **2014**, *5*, 3473.

[29] W. Xue, W. Xiao, J. Shang, X. X. Chen, X. J. Zhu, L. Pan, H. W. Tan, W. B. Zhang, Z. H. Ji, G. Liu, X.-H. Xu, J. Ding, R.-W. Li, *Nanotechnology* **2014**, *25*, 425204.

[30] Y. J. Fu, F. J. Xia, Y. L. Jia, J. Y. Li., X. H. Dia, G. S. Fu, B. Y. Zhu, B. T. Liu, *Appl. Phys. Lett.* **2014**, *104*, 223505.

[31] M. Morales-Masis, S. J. van der Molen, W. T. Fu, M. B. Hesselberth, J. M. van Ruitenbeek, *Nanotechnology* **2009**, *20*, 095710.

[32] S. Gao, C. Song, C. Chen, F. Zeng, F. Pan, *J. Phys. Chem. C* **2012**, *116*, 17955.

[33] C. B. Lee, B. S. Kang, A. Benayad, M. J. Lee, S.-E. Ahn, K. H. Kim, G. Stefanovich, Y. Park, I. K. Yoo, *Appl. Phys. Lett.* **2008**, *93*, 042115.

[34] J. Huang, D. Ma, *Appl. Phys. Lett.* **2014**, *105*, 093303.

[35] S. ChandraKishore, A. Pandurangan, *R. Soc. Chem. Adv.* **2014**, *4*, 9905.

[36] M.-J. Lee, C. B. Lee, D. Lee, S. R. Lee, M. Chang, J. H. Hur, Y.-B. Kim, C.-J. Kim, D. H. Seo, S. Seo, U.-I. Chung, I.-K. Yoo, K. Kim, *Nat. Mater.* **2011**, *10*, 625.

[37] X. He, X. Li, *Appl. Phys. Lett.* **2013**, *102*, 221601.

[38] D. I. Son, T. W. Kim, J. H. Shim, J. H. Jung, D. U. Lee, J. M. Lee, W. I. Park, W. K. Choi, *Nano Lett.* **2010**, *10*, 2441.

[39] A. A. Bessonov, M. N. Kirikova, D. I. Petukhov, M. Allen, T. Ryhänen, M. J. A. Bailey, *Nat. Mater.* **2015**, *14*, 199.

[40] T. Sakamoto, H. Sunamura, H. Kawaura, T. Hasegawa, T. Nakayama, M. Aono, *Appl. Phys. Lett.* **2003**, *82*, 3032.

[41] J. Chen, D. Ma, *J. Appl. Phys.* **2006**, *100*, 034512.

[42] R. Soni, P. Meuffels, A. Petraru, M. Weides, C. Kügeler, R. Waser, H. Kohlstedt, *J. Appl. Phys.* **2010**, *107*, 024517.

[43] B. J. Choi, D. S. Jeong, S. K. Kim, C. Rohde, S. Choi, J. H. Oh, H. J. Kim, C. S. Hwang, K. Szot, R. Waser, B. Reichenberg, S. Tiedke, *J. Appl. Phys.* **2005**, *98*, 033715.

[44] S.-L. Li, D. Shang, J. Li, J. Gang, D. Zheng, *J. Appl. Phys.* **2009**, *105*, 033710.

[45] K. Szot, W. Speier, G. Bihlmayer, R. Waser, *Nat. Mater.* **2006**, *5*, 312.

[46] M. Hasan, R. Dong, H. J. Choi, D. S. Lee, D.-J. Seong, M. B. Pyun, H. Hwang, *Appl. Phys. Lett.* **2008**, *92*, 202102.

[47] H. J. Snaith, A. Abate, J. M. Ball, G. E. Eperon, T. Leijtens, N. K. Noel, S. D. Stranks, J. T.-W. Wang, K. Wojciechowski, W. Zhang, *J. Phys. Chem. Lett.* **2014**, *5*, 1511.

[48] J. M. Azpiroz, E. Mosconi, J. Bisquert, F. De Angelis, *Energy Environ. Sci.* **2015**, *8*, 2118.

[49] E. L. Unger, E. T. Hoke, C. D. Bailie, W. H. Nguyen, A. R. Bowring, T. Heumüller, M. G. Christoforo, M. D. McGehee, *Energy Environ. Sci.* **2014**, *7*, 3690.

[50] D. A. Egger, E. Edri, D. Cahen, G. Hodes, *J. Phys. Chem. Lett.* **2015**, *6*, 279.

[51] A. Walsh, D. O. Scanlon, S. Chen, X. Gong, S. H. Wei, *Angew. Chem.* **2014**, *53*, 1.

[52] W. J. Yin, T. T. Shi, Y. F. Yan, *J. Phys. Chem. C* **2015**, *119*, 5253.

[53] Z. Zhang, Q. Ge, S.-C. Li, B. D. Kay, J. M. White, Z. Dohnálek, *Phys. Rev. Lett.* **2007**, *99*, 126105.

[54] B. P. Uberuaga, L. J. Vernon, *Solid State Ion.* **2013**, *253*, 18.